Solid State Communications 246 (2016) 29–32

Contents lists available at ScienceDirect

Solid State Communications

journal homepage: www.elsevier.com/locate/ssc

Fast-track communication

Temperature and field dependence of the flux pinning mechanisms in $Fe_{1.06}Te_{0.6}Se_{0.4}$ single crystal

S.J. Hossaini [a], S.R. Ghorbani [a,*], H. Arabi [a], X.L. Wang [b], C.T. Lin [c]

[a] Department of Physics, Ferdowsi University of Mashhad, Mashhad, Iran
[b] Institutes for Superconducting and Electronic Materials, Australian Institute for Innovative Materials, University of Wollongong, Faculty of Engineering, North Wollongong, NSW 2519, Australia
[c] Max-Planck-Institut für Festkörperforschung, Heisenbergstr. 1, 70569 Stuttgart, Germany

ARTICLE INFO

Article history:
Received 11 June 2016
Received in revised form
27 July 2016
Accepted 28 July 2016
Available online 29 July 2016

Keywords:
A. $Fe_{1.06}Te_{0.6}Se_{0.4}$ single crystal
B. Critical current density
C. Flux pinning mechanism

ABSTRACT

The temperature and magnetic field dependence of the magnetization and critical current density of $Fe_{1.06}Te_{0.6}Se_{0.4}$ single crystal have been investigated, and the flux pinning mechanism has been analyzed. The critical current density results indicate that there are different pinning mechanisms in this crystal. The pinning mechanisms are studied in terms of the pinning model where the normalized volume pinning force, f_p, versus $h = H/H_{irr}$, where H_{irr} is the irreversibility, were studied systematically. It was found that a variety of pinning mechanisms including normal point pinning, normal surface pinning, and pinning based on spatial variation in the Ginzburg-Landau parameter (Δk pinning) pinning mechanisms coexist. The effects each of the different pinning mechanisms were obtained. The results show that the contributions of the real pinning mechanisms are dependent on the temperature and magnetic field in this the single crystal.

1. Introduction

The discovery of $LaO_{1-x}F_xFeAs$, a superconductor with a transition temperature of 26 K, led to the exciting study of non-cuprate high-temperature superconductors [1]. Soon afterwards, this discovery led to the identification of iron-based superconductor families with different crystal structures, generally referred to as "1111" for $REFeAs(O, F)$ (RE = *rare earth elements*), "122" for $AEFe_2As_2$ (AE = alkaline earth elements) [2] and $AEFe_2Se_2$ [3], "111" for $LiFeAs$ [4] and "11" for $Fe(Se, Te)$ [5]. These superconductors have attracted great interest because of their multiband features [6,7], unconventional pairing symmetry [8,9], and potential for applications.

Among the Fe-based superconductors, the compounds have been a good candidate for understanding the real mechanism of superconductivity, because of the relatively simple structure and similarity in the Fermi surface (E_F) of this class of compounds. The Fermi surfaces of $FeSe$ and $FeTe$ contains cylindrical sections for holes and electrons at the center and at the corners of the Brillouin zone, respectively. $FeSe$ has a superconducting transition temperature (T_c) at 8 K, which rises to 14.5 K for 60% substitution of Te at Se sites [10,11].

In this work, the critical current density of $Fe_{1.06}Te_{0.6}Se_{0.4}$ single crystal has studied by measurements of the magnetization as a function of magnetic field at different temperatures. The pinning mechanisms were analyzed by two models in terms of the different pinning effects. The results indicated that a variety of pinning mechanisms, e.g. normal point pinning, normal surface pinning, and Δk pinning, coexist in $Fe_{1.06}Te_{0.6}Se_{0.4}$ single crystal. The results show that the contributions of the pinning mechanisms depend on both the temperature and the magnetic field.

2. Experiments

Single crystal of $Fe_{1.06}Te_{0.6}Se_{0.4}$ was prepared by a self-flux method. Details of the single crystal growth are reported elsewhere [12]. The as-grown single crystal was cleaved and cut into a rectangular shape for magnetic measurements. The magnetization was measured over a wide range of temperatures and magnetic fields up to 13 T with applied current of 5 mA, using a physical properties measurement system (PPMS, Quantum Design). The critical current density was calculated by using the Bean approximation.

* Corresponding author.
E-mail address: sh.ghorbani@um.ac.ir (S.R. Ghorbani).

http://dx.doi.org/10.1016/j.ssc.2016.07.030
0038-1098/

3. Results and discussion

Fig. 1 shows a typical hysteresis (M–H) loops measured in positive magnetic fields along the $H\|c$ direction up to 13 T at several temperatures below T_c. The maximum in the absolute value of the magnetization located at or near zero field represents the first magnetization peak. The field penetrates through the bulk of the sample completely after zero field cooling [13]. At low magnetic field, the magnetization decreases as the magnetic field increases, but at intermediate fields it shows a broad maximum again, which is denoted as the second peak, and it finally diminishes to zero at higher fields.

The appearance of the second peak is known as the fishtail effect, and it has also been observed for single crystals of LaSrCuO [14], $YBa_2Cu_3O_y$ [15], BaSrCaCuO (BSCCO), and more recently in Ba $(Fe_{0.93}Co_{0.07})_2As_2$ [16], $FeTe_{0.6}Se_{0.4}$ [17] and $Fe_{1.04}Te_{0.6}Se_{0.4}$ [18]. Although the origin of this behavior is not precisely specified as yet, it was suggested that it may occur due to the presence of some weakly superconducting or non-superconducting regions that can act as the efficient pinning centers [15,19]. It was also suggested that the crossover from single vortex pinning to collective flux creep induces slower magnetic relaxation at intermediate fields and gives rise to the second peak [15,16,19]. As can be seen in Fig. 1, the peak onset (H_{sp}^{onset}) and peak (H_{sp}^{peak}) positions move to lower magnetic fields as temperature increases.

The critical current density J_c was obtained from the width of the magnetization loop, ΔM. According to the Bean model, the critical current density $J_c(T, H)$ can be calculated from $J_c=20\Delta M/Va(1-a/3b))$ for a rectangular shaped crystal with H||c where a and b are the dimensions of the sample perpendicular to the applied magnetic field, with $a<b$ and V is the volume the sample, and ΔM is the height of the M–H hysteresis loop [20].

Fig. 2 shows J_c versus magnetic field. As can be seen in Fig. 2, the fishtail effect is observed to be more obvious than in Fig. 1. The $J_c(H\sim0, T)$ at 2 K and 4 K is 2.65×10^5 A/cm^2 and 1.4×10^5 A/cm^2, respectively. These values are larger than the reported values, 1.0×10^5 A/cm^2 for Fe $Te_{0.6}Se_{0.4}$ single crystal at $T=1.8$ K, and 1.2×10^5 A/cm^2 for $Fe_{1.04}Te_{0.6}Se_{0.4}$ single crystal at 4 K [17,18]. This increase in critical current density may be attributed to the excess iron concentration, which introduces more defects or pinning centers into the crystal structure, and consequently, higher pinning potential into the system [18]. Although increasing the Fe concentration results in an increased J_c, it decreases not only the T_c, but also the superconducting volume fraction of the sample [21]. It was reported that annealing in O_2 and I_2 de-intercalates the

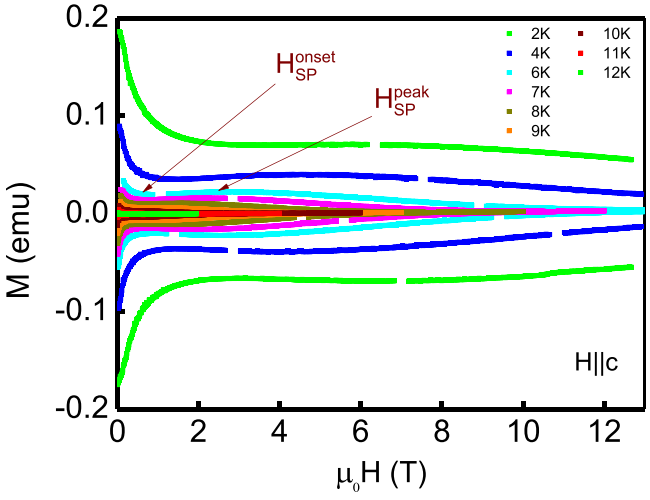

Fig. 1. M–H loops of $Fe_{1.06}Te_{0.6}Se_{0.4}$ single crystal at different temperatures from 2 to 12 K.

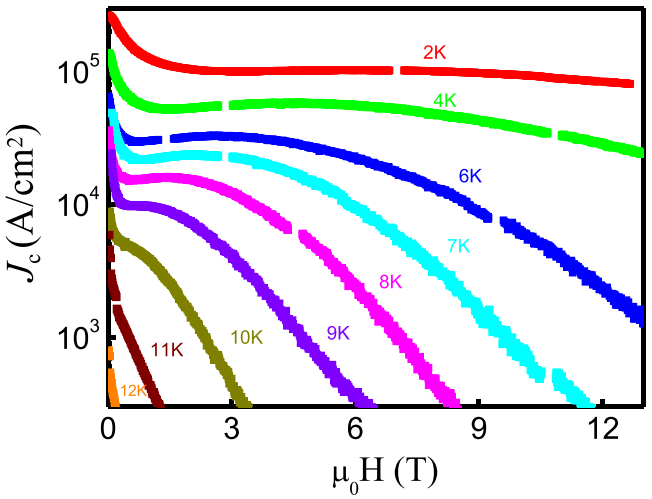

Fig. 2. The critical current density J_c vs. magnetic field at temperatures ranging from 2 to 12 K.

Fe excess form the inner part of $Fe_{1+y}Te_{0.6}Se_{0.4}$ single crystals, and this induces bulk superconductivity in the single crystals [22]. Therefore, the excess Fe concentration strongly affects the superconductivity properties of $Fe_{1+y}Te_{0.6}Se_{0.4}$ samples [23,24].

The flux pinning force density was calculated by $|\boldsymbol{F_p}| = |\boldsymbol{\mu_0 H} \times \boldsymbol{J}|$. In order to understand the real flux pinning mechanism effects over the whole field range, the normalized volume pinning force was scaled by the common law of $f = Ah^p(1-h)^q$ [25], where A is a coefficient associated with the material properties of the sample, p and q are parameters that depend on the pinning mechanisms, and $h=H/H_{irr}$, where H_{irr} is the irreversibility field, which is obtained by using the criterion of $J_c=100$ A/cm^2. In this model, $p=1$ and $q=1$ describes volume Δk pinning (KP), $p=1$ and $q=2$ normal point pinning (NPP), and $p=0.5$ and $q=2$ normal surface pinning (NSP) mechanism. The maximum of F_p is

$$F_{p,max}=A[h^p(1-h)^q]_{max} \tag{1}$$

Therefore,

$$f_p(h)=\frac{F_p}{F_{p,max}}=\frac{Ah^p(1-h)^q}{A[h^p(1-h)^q]_{max}}=\frac{h^p(1-h)^q}{[h^p(1-h)^q]_{max}} \tag{2}$$

where the maximum of $f_p(h)$ occurs at $h_{max}=p/(p+q)$.

For obtaining the real pinning effect contributions based on Eq. (2), which is used by considering the existence of the volume Δk pinning, f_{KP}, the normal point pinning, f_{NPP}, and the normal surface pinning, f_{NSP} mechanisms within the following equation:

$$f=b_k f_{KP}+b_p f_{NPP}+b_s f_{NSP} \tag{3}$$

where b_p, b_s, and b_k are fitting parameters, which indicate the KP, NPP and NSP effects, respectively, with $b_p+b_s+b_k=1$. The dashed and solid-curves in the inset of Fig. 3 shows an example of the scaling of Eqs. (2) and (3), respectively, to the experimental data at 9 K.

The normalized flux pinning force density versus the reduced magnetic field (h) is plotted in Fig. 3 at different temperatures. The position of the maximum in the experimental data moves towards lower reduced magnetic fields, h, as the temperature increases. This indicates that the pinning mechanism effect depends on temperature. Theoretical curves related to the KP, NPP, and NSP pinning mechanisms are also plotted in Fig. 3 by dashed-curves. As can be seen in Fig. 3, the experimental data located between the theoretical curves related to different pinning mechanisms, where the location of the maximum in the experimental data depends on temperature. At reduced magnetic fields smaller than 0.37,

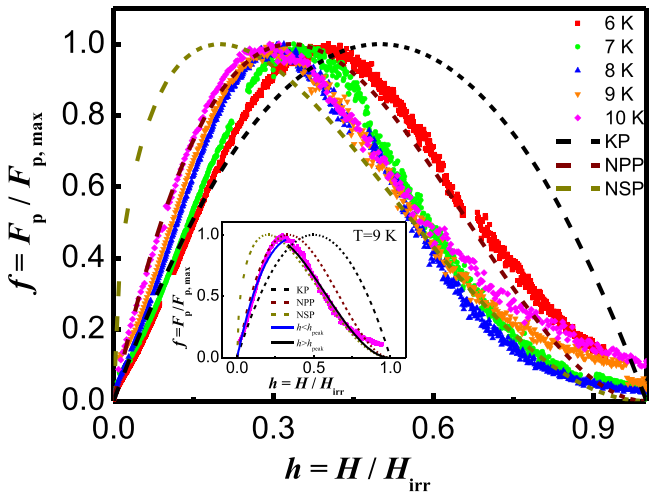

Fig. 3. Field dependence of the normalized pinning force, with the fitting results obtained from $h^p(1-h)^q$. Inset shows an example of the scaling of Eqs. (2) and (3) to the experimental data at 9 K.

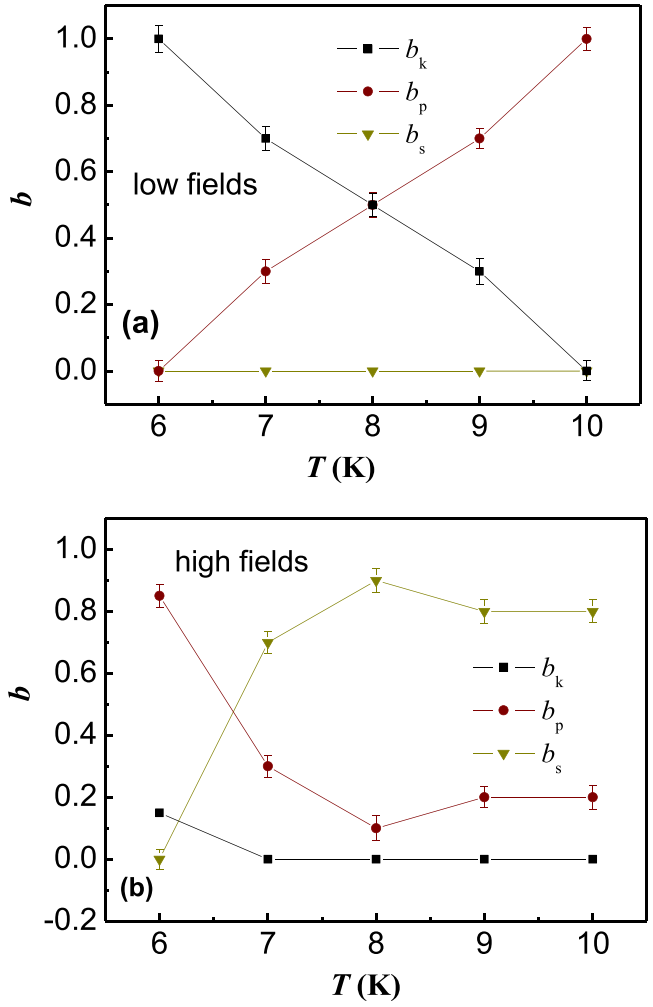

Fig. 4. Temperature dependence of b_k,b_p, and b_s in (a) the low field region ($h < h_{peak}$) and (b) the high field region ($h > h_{peak}$). The error bar illustrates estimated the uncertainty of parameters.

$h < 0.37$, the experimental data located between the two curves corresponding to the KP and NPP mechanisms. As the temperature increases, the peak of the experimental data comes towards to the NPP curve and finally the peak corresponding to 10 K locates in the position of the theoretical curve corresponding to the NPP mechanism. This shows that at $h < h_{peak}$, the dominant pinning must be due to both the KP and the NPP mechanisms and that their contributions are dependent on temperature. While at the reduced magnetic field larger than h_{peak}, $h > h_{peak}$, the NSP mechanism also may be taken into account in addition to the KP and NPP pinning effects.

The contributions of each pinning mechanism for both the $h < h_{peak}$ (low fields) and the $h > h_{peak}$ (high fields) regions are shown in Fig. 4 at different temperatures. At low fields, the results show that the KP mechanism is the dominant mechanism at temperatures below 8 K. As the temperature increases, its contribution gradually decreases and the NPP mechanism is enhanced up to 10 K, where the volume Δk, KP, mechanism is suppressed completely. It was also found that there was no contribution for the NSP pinning mechanism. However, at high magnetic field (Fig. 4b) as temperature increases the NPP mechanism contribution decreases and the NSP pinning mechanism plays a major role. In this region, there is no effect from the volume Δk pinning mechanism, KP, at temperatures above 7 K. Almost the same pinning-mechanism temperature dependence was observed in nano-Si and $SiCl_4$ doped MgB_2 samples [26]. It was reported the coexistance of both the NPP and the NSP mechanisms for $FeTe_{0.6}Se_{0.4}$ [27] and for $Fe_{1.04}Te_{0.6}Se_{0.4}$ [18] single crystals.

4. Conclusions

The critical current density J_c of $Fe_{1.06}Te_{0.6}Se_{0.4}$ single crystal was calculated by using M–H loops. The J_c results suggest that excess Fe improves the pinning potential and results in enhancement of the J_c. The pinning mechanisms were studied in this single crystal by the Dew-Hughes [26] model in terms of the different pinning effects. The results indicated that a variety of pinning mechanisms, e.g. normal point pinning, normal surface pinning, and Δk pinning coexist in $Fe_{1.06}Te_{0.6}Se_{0.4}$ single crystal. The results show that the contribution of the pinning mechanisms depend on both the temperature and the magnetic field.

Acknowledgments

The work was supported by the Ferdowsi University of Mashhad (Grant no. 39734).

References

[1] Y. Kamihara, T. Watanabe, M. Hirano, H. Hosono, J. Am. Chem. Soc. 130 (2008) 3296.
[2] M. Rotter, M. Tegel, D. Johrendt, I. Schellenberg, W. Hermes, R. Pottgen, Phys. Rev. B 78 (2008) 020503 (R).
[3] J. Guo, S. Jin, G. Wang, S. Wang, K. Zhu, T. Zhou, M. He, X. Chen, Phys. Rev. B 82 (2010) 180520 (R).
[4] X.C. Wang, Q.Q. Liu, Y.X. Lv, W.B. Gao, L.X. Yang, R.C. Yu, F.Y. Li, C.Q. Jin, Solid State Commun. 148 (2008) 538.
[5] F.C. Hsu, J.Y. Luo, K.W. Yeh, T.K. Chen, T.W. Huang, P.M. Wu, Y.C. Lee, Y.L. Huang, Y.Y. Chu, D.C. Yan, M.K. Wu, Proc. Natl. Acad. Sci. USA 105 (2008) 14262.
[6] F. Hunte, J. Jaroszynski, A. Gurevich, D.C. Larbalestier, R. Jin, A.S. Sefat, M. A. McGuire, B.C. Sales, D.K. Christen, D. Mandrus, Nature 453 (2008) 903.
[7] X. Zhu, H. Yang, L. Fang, G. Mu, H.H. Wen, Supercond. Sci. Technol. 21 (2008) 105001.
[8] L. Shan, Y. Wang, X. Zhu, Gang Mu, L. Fang, C. Ren, H.H. Wen, Eur. Phys. Lett. 83 (2008) 57004.
[9] K. Seo, C. Fang, B.A. Bernevig, J. Hu, Phys. Rev. B 79 (2008) 235207.
[10] M.H. Fang, H.M. Fam, B. Qian, T.J. Liu, E.K. Vehstedt, Y. Liu, L. Spinu, Z.Q. Mao, Phys. Rev. B 78 (2008) 224503.
[11] A. Subedi, L. Zhang, D.J. Singh, M.H. Du, Phys. Rev. B 78 (2008) 134514.
[12] Y. Liu, C.T. Lin, J. Supercond. Nov. Magn. 24 (2011) 183.
[13] P. Das, A.D. Thakur, A.K. Yadav, C.V. Tomy, M.R. Lees, G. Balakrishnan, S. Ramakrishnan, A.K. Grover, Phys. Rev. B 84 (2011) 214526.

[14] Y.V. Bugoslavsky, A.L. Ivanov, A.A. Minakov, S.I. Vasyurin, Physica C 233 (1994) 67.
[15] C.D. Wei, Z.X. Liu, H.T. Ren, L. Xiao, Physica C 260 (1996) 130.
[16] R. Prozorov, N. Ni, M.A. Tanatar, V.G. Kogan, R.T. Gordon, C. Martin, E. C. Blomberg, P. Prommapan, J.Q. Yan, S.L. Bud'ko, P.C. Canfield, Phys. Rev. B 78 (2008) 224506.
[17] C.S. Yadav, P.L. Paulose, New J. Phys. 11 (2009) 103046.
[18] M. Shahbazi, X.L. Wang, S.X. Dou, H. Fang, C.T. Lin, J. Appl. Phys. 113 (2013) 17E115.
[19] L. Krusin-Elbaum, L. Civale, V.M. Vinokur, F. Holtzberg, Phys. Rev. Lett. 69 (1992) 2280.
[20] C.P. Bean, Rev. Mod. Phys. 36 (1964) 31.
[21] T.J. Liu, X. Ke, B. Qian, J. Hu, D. Fobes, E.K. Vehstedt, H. Pham, J.H. Yang, M. H. Fang, L. Spinu, P. Schiffer, Y. Liu, Z.Q. Mao, Phys. Rev. B 80 (2009) 174509.
[22] Y. Sun, T. Taen, Y. Tsuchiya, Z.X. Shi, T. Tamegai, Supercond. Sci. Technol. 26 (2013) 015015.
[23] W. Bao, Y. Qiu, Q. Huang, M.A. Green, P. Zajdel, M.R. Fitzsimmons, M. Zhernenkov, S. Chang, M. Fang, B. Qian, E.K. Vehstedt, J. Yang, H.M. Pham, L. Spinu, Z.Q. Mao, Phys. Rev. Lett. 102 (2009) 247001.
[24] M. Bendele, P. Babkevich, S. Katrych, S. Gvasaliya, E. Pomjakushina, K. Conder, B. Roessli, A.T. Boothroyd, R. Khasanov, H. Keller, Phys. Rev. B 82 (2010) 212504.
[25] D. Dew-Hughes, Philos. Mag. 30 (1974) 293.
[26] S.R. Ghorbani, M. Hosseinzadeh, X.L. Wang, Supercond. Sci. Technol. 28 (2015) 125006.
[27] C.S. Yadav, P.L. Paulose, Solid State Commun. 151 (2011) 216.